



Published in final edited form as:

Int J Comput Assist Radiol Surg. 2020 January ; 15(1): 87–98. doi:10.1007/s11548-019-02023-y.

Normative ranges of nasal airflow variables in healthy adults

Azadeh A.T. Borojeni, PhD^{1,2,*}, Guilherme J. M. Garcia, PhD^{1,2,*}, Masoud G. Moghaddam, PhD^{1,2}, Dennis O. Frank-Ito, PhD^{3,4,5}, Julia S. Kimbell, PhD⁶, Purushottam W. Laud, PhD⁷, Lisa J. Koenig, BChD, DDS, MS⁸, John S. Rhee, MD MPH¹

¹Department of Otolaryngology and Communication Sciences, Medical College of Wisconsin, Milwaukee, WI

²Department of Biomedical Engineering, Marquette University & The Medical College of Wisconsin, Milwaukee, WI

³Division of Head and Neck Surgery & Communication Sciences, Duke University Medical Center, Durham, NC

⁴Computational Biology & Bioinformatics Program, Duke University, Durham, NC, USA

⁵Department of Mechanical Engineering and Materials Science, Duke University, Durham, NC

⁶Department of Otolaryngology/Head and Neck Surgery, University of North Carolina School of Medicine, Chapel Hill, NC

⁷Institute for Health and Society, Division of Biostatistics, Medical College of Wisconsin, Milwaukee, WI

⁸Department of Oral Medicine and Oral Radiology, Marquette University School of Dentistry, Milwaukee, WI

Abstract

Purpose: Virtual surgery planning based on computational fluid dynamics (CFD) simulations of nasal airflow has the potential to improve surgical outcomes for patients with nasal airway obstruction (NAO). Virtual surgery planning requires normative ranges of airflow variables, but few studies to date have quantified inter-individual variability of nasal airflow among healthy subjects. This study reports CFD simulations of nasal airflow in 47 healthy adults.

Methods: Anatomically-accurate 3-dimensional nasal models were reconstructed from cone beam computed tomography (CBCT) scans and used for steady-state inspiratory airflow

Corresponding author: Guilherme J.M. Garcia, Department of Biomedical Engineering, Department of Otolaryngology and Communication Sciences, Medical College of Wisconsin, 8701 Watertown Plank Road, Milwaukee, WI 53226, Phone: 414-955-4466 / Fax: 414-955-6568, ggarcia@mcw.edu.

*These authors contributed equally to this paper.

Publisher's Disclaimer: This Author Accepted Manuscript is a PDF file of an unedited peer-reviewed manuscript that has been accepted for publication but has not been copyedited or corrected. The official version of record that is published in the journal is kept up to date and so may therefore differ from this version.

Conflict of Interest: The authors declare that they have no conflict of interest.

Ethical Approval: All procedures were performed in accordance with the ethical standards of the institutional review boards at The Medical College of Wisconsin and Marquette University and of the 1964 Helsinki declaration and its later amendments.

Informed Consent: Informed consent was obtained from all individual participants included in the study.

simulations with a bilateral flowrate of 250 ml/s. Normal subjective sensation of nasal patency was confirmed using the Nasal Obstruction Symptom Evaluation (NOSE) and Visual Analog Scale (VAS). Healthy ranges for several CFD variables known to correlate with subjective nasal patency were computed, including unilateral airflow, nasal resistance, airspace minimal cross-sectional area (mCSA), heat flux (HF), and surface area stimulated by mucosal cooling (defined as the area where $HF > 50 \text{ W/m}^2$). The normative ranges were targeted to contain 95% of the healthy population and computed using a non-parametric method based on order statistics.

Results: A wide range of interindividual variability in nasal airflow was observed among healthy subjects. Unilateral airflow varied from 60 ml/s to 191 ml/s, airflow partitioning ranged from 23.8% to 76.2%, and unilateral mCSA varied from 0.24 cm^2 to 1.21 cm^2 . These ranges are in good agreement with rhinomanometry and acoustic rhinometry data from the literature. A key innovation of this study are the normative ranges of flow variables associated with mucosal cooling, which recent research suggests is the primary physiological mechanism of nasal airflow sensation. Unilateral HF ranged from 94 to 281 W/m^2 , while the surface area stimulated by cooling ranged from 27.4 to 64.3 cm^2

Conclusions: These normative ranges may serve as targets in future virtual surgery planning for patients with NAO.

Keywords

Nasal airway obstruction (NAO); virtual surgery planning; computational fluid dynamics (CFD) simulations of nasal airflow; normative range in healthy subjects; mucosal cooling in nasal cavity

INTRODUCTION

The clinical value of objective measures of nasal obstruction remains controversial. Rhinologists are divided into two groups, those who advocate for using objective measures in clinical practice (such as rhinomanometry, acoustic rhinometry, and peak nasal inspiratory flow) and those who are skeptical of their clinical value [1–6]. There is some evidence that success rates of nasal surgery can be improved when objective measures are used in surgical planning [7]. However, the low correlation between traditional objective measures and subjective sensation of nasal airflow remains a significant challenge that prevents universal adoption of traditional techniques in clinical care [2].

Virtual surgery planning based on computational fluid dynamics (CFD) simulations has the potential to better correlate with subjective perception of nasal airflow than traditional techniques. The reasons to be optimistic about clinical application of CFD-based virtual surgery planning are three-fold. First, recent research suggests that the primary physiological mechanism for sensing nasal airflow is the activation of menthol-sensitive TRPM8 cold receptors [8,9]. Objective methods to quantify mucosal cooling *in vivo* are lacking [9]. Our group [10–13] and others [14,15] have shown that CFD-derived measures of mucosal cooling correlate with subjective sensation of nasal airflow. Since CFD variables correlate strongly with each other, the same studies also reported a correlation between subjective perception of nasal airflow and other CFD variables, such as nasal resistance [10] and intranasal airflow distribution [13]. Additional studies are needed to determine which CFD

variable will be the most useful for clinical applications. Second, a systematic literature review found that subjective perception of nasal airflow has a better correlation with unilateral airflow than with bilateral airflow [2]. Similarly, our group reported that unilateral CFD variables have a stronger correlation with subjective scores of nasal airflow than bilateral CFD variables [10]. We believe that this partially explains the lack of correlation between subjective perception and traditional objective measures of nasal airflow. Finally, a major strength of CFD-based virtual surgery planning is the ability to predict how anatomical changes will affect nasal airflow [16,17].

Many studies have investigated nasal airflow in humans using *in vitro* experiments or computer simulations [18–22]. However, the vast majority of these studies were limited to small cohorts, typically from 1 to 5 subjects. Notable exceptions are the pioneering studies by Zhao and Jiang [23], Ramprasad and Frank-Ito [24], and Sanmiguel-Rojas and colleagues [25] who investigated nasal airflow in cohorts of 22, 16, and 24 healthy adults, respectively. Due to significant inter-individual variability in the nasal cavity anatomy [26–28], there is a need to quantify inter-individual variability in nasal airflow variables in larger cohorts, so that normative ranges can be established. This study aims to extend previous works in the literature by using computational fluid dynamics to quantify nasal airflow characteristics in 47 healthy adults. One innovation of this work is that we report normative ranges for the airspace minimal cross-sectional area and the surface area stimulated by mucosal cooling, which were not investigated in past CFD studies of healthy adults.

Many hospitals have databases of computed tomography (CT) scans of patients. One strategy to create a cohort of CFD models of healthy individuals is to have board-certified otolaryngologists screen these databases to identify patients with a normal nasal anatomy [24,25]. Although readily available, information contained in CT scans from these databases may not be sufficient to rule out nasal symptoms. This is problematic because otolaryngologists often see patients with normal CT images who still complain of nasal symptoms. A recent systematic literature review found that subjects in the general population have higher scores of subjective nasal obstruction than subjects in cohorts evaluated as healthy [29]. In the present study, healthy volunteers were prospectively recruited from a dental clinic and deemed to have a normal nasal anatomy based on history, subjective scores of nasal patency, and CT findings.

Surgery to treat nasal airway obstruction (NAO) has a relatively high failure rate [30–35]. Virtual surgery planning based on CFD simulations has the potential to improve surgical outcomes [16,36–38]. Comparison of CFD variables in NAO patients with normative ranges can provide objective criteria to select which patients are most likely to benefit from surgery and to select the optimal surgical procedure for each patient. The aim of this study is to quantify the nasal airflow characteristics in healthy adults and provide normative ranges that can serve as targets for future NAO virtual surgery planning.

METHODS

Cohort demographics

This study was approved by the Institutional Review Board (IRB) committees of both Marquette University and The Medical College of Wisconsin under protocol PR022934. A cohort of 55 healthy subjects were prospectively enrolled at the Marquette University Oral Medicine and Oral Radiology clinic. Subjects scheduled to undergo imaging of the maxilla as part of their dental treatment were invited to participate in the study. The inclusion criteria were age ≥ 18 years, no history of nasal surgery, no symptoms of nasal obstruction, and non-smoker status. Patients who were pregnant and patients with a history of nasal surgery, severe nasal trauma resulting in a crooked nose, autoimmune disease, chronic sinusitis, severe allergies, or other sinonasal disease were excluded. After initial screening with a questionnaire, subjects who fulfilled the inclusion criteria completed the informed consent process with the radiologist, which emphasized the voluntary nature of participation. Informed consent was obtained from all individual participants included in the study.

Subjects were administered two self-reported surveys of nasal patency, the nasal obstruction symptom evaluation (NOSE) [39] and a double ordinal visual analog scale (VAS), ranging from 0–10, for assessment of nasal patency. The NOSE scale is a disease-specific quality of life instrument that provides a score ranging from 0 (no symptoms of NAO) to 100 (severe symptoms of NAO) [39]. To obtain unilateral VAS scores, participants were asked to cover one nostril and rate their ability to breathe through the uncovered nostril on a 0 (no obstruction) to 10 (severe obstruction) scale. This was repeated for each nostril.

Cone beam computed tomography (CBCT) scans of the nasal cavity were obtained from 55 healthy subjects. After the scans were reviewed by an otolaryngologist, 3 subjects were excluded because their CBCT scans showed signs of sinusitis. Furthermore, 5 subjects were excluded for having NOSE score > 32 . The cutoff value of 32 was based on the mean NOSE score plus one standard deviation of healthy subjects (i.e., $15 + 17 = 32$) in a recent systematic literature review performed by our group [29]. Thus, the final cohort included 47 healthy subjects with no history of nasal disease, a normal anatomy on the CBCT scan as assessed by a board-certified otolaryngologist, and no subjective feeling of nasal obstruction (Fig. 1 and Fig. S1 in the Electronic Supplementary Material). The cohort had a mean age of 48 ± 18 years (range: 18 to 81 years, median: 52 years). It included 19 males and 28 females: 35 Caucasians, 1 Native American, 2 African Americans, 5 Hispanics, 3 Asians, and 1 patient who self-identified as other ethnicity (Table S1 in the Electronic Supplementary Material).

It is important to note that the presence of a septal deviation was not considered to be an exclusion criterion. Studies of cranial computed tomography scans reveal that 20% to 26% of healthy adults have a septal deviation [40–44]. Therefore, many septal deviations are asymptomatic. Our exclusion criterion was based on the current gold-standard measure of subjective perception of nasal obstruction, namely the NOSE score [39,45]. As described above, subjects with NOSE score > 32 were excluded.

Reconstruction of nasal airway models

Anatomically accurate 3-dimensional (3D) reconstructions of the nasal cavities were created from the CBCT scans (Fig. 2). The CBCT scans were imported to the medical imaging package Mimics™ 17.0 (Materialise Inc, Leuven, Belgium). A threshold range of -1024 to -300 Hounsfield Units (HU) was set to segment the airspace from the nostrils to the nasopharynx. The paranasal sinuses were excluded manually. The motivation for excluding the paranasal sinuses is three-fold. First, airflow into the sinuses is negligible compared to airflow through the main nasal passages. Second, inclusion of the paranasal sinuses would make it very challenging to quantify intranasal airflow distribution into inferior, middle, and superior regions. Third, inclusion of the paranasal sinuses would require larger mesh sizes and computational times. For these reasons, most CFD studies of nasal airflow exclude the paranasal sinuses, except when the goal is to quantify sinus airflow.

In 21 subjects, the field of view during CBCT imaging was limited to minimize radiation dose and thus the nasopharynx was excluded from the scans (Fig. 2B). In these models, an idealized nasopharynx was employed for outlet boundary conditions. Validation of the idealized nasopharynx was performed in a previous study [46], which demonstrated that use of an idealized nasopharynx had a negligible effect on the inspiratory airflow patterns in the nasal cavity. The nasal airway geometry was exported from Mimics™ in stereolithography (STL) format, and then imported into ICEM-CFD™ 14.0 (ANSYS, Canonsburg, PA), where unstructured meshes with approximately 4 million tetrahedral cells were created.

Numerical methods and boundary conditions

Steady-state inspiratory nasal airflow simulations were performed using numerical methods described previously [10,47], Briefly, nasal airflow is governed by the Navier-Stokes and continuity equations

$$\rho \frac{\partial \mathbf{u}}{\partial t} + \rho(\mathbf{u} \cdot \nabla)\mathbf{u} = -\nabla p + \mu \nabla^2 \mathbf{u} \quad (1)$$

$$\nabla \cdot \mathbf{u} = 0 \quad (2)$$

where $\mathbf{u} = \mathbf{u}(x,y,z,t)$ is the air velocity vector, $\rho = 1.204 \text{ kg/m}^3$ is the air density, $\mu = 1.825 \times 10^{-5} \text{ kg/(m.s)}$ is the dynamic viscosity of air, p is pressure and t is time. For the CFD simulations presented here, airflow was assumed to be steady and laminar. The assumption that nasal airflow is laminar for resting breathing is supported by experiments [19,22].

Heat transfer in the nasal cavity was quantified by solving the heat equation

$$\frac{\partial T}{\partial t} + (\mathbf{u} \cdot \nabla)T = \frac{k}{\rho C_p} \nabla^2 T \quad (3)$$

where T is temperature, $C_p = 1005.9 \text{ J/Kg-K}$ is specific heat of air, and $k = 0.0268 \text{ W/m-K}$ is the thermal conductivity of air.

The numerical simulations were conducted using the finite volume method as implemented in ANSYS Fluent™ 14.0 (ANSYS, Inc.). A second-order upwind scheme was used for discretization. A segregated solver was implemented, and the SIMPLEC algorithm was used to couple the pressure and velocity fields.

Nasal walls were assumed rigid and the no-slip velocity condition was applied. At the nostrils, an inlet pressure boundary condition was applied with zero gauge pressure.¹ For heat transfer simulations, $T = 20^{\circ}\text{C}$ was set at the nostrils. A value of $T = 32.6^{\circ}\text{C}$, based on experimental measurements by Lindemann and colleagues [49], was used as the average nasal mucosal temperature during inhalation.

A bilateral flowrate of 250 ml/s, which represents an adult breathing at rest [50], was used in all subjects. This flowrate was obtained by adjusting the outlet pressure while keeping the inlet pressure at the nostrils equal to atmospheric pressure. The outlet pressure required to reach a bilateral flowrate of 250 ml/s was determined by running preliminary simulations to quantify the relationship between outlet pressure and flow rate, which was fitted with the power law $P_{outlet} = aQ^b$, where P_{outlet} is the outlet pressure, Q is the bilateral flowrate, and a and b are fitted constants.

Objective measures of nasal airflow

Several CFD variables known to correlate with subjective nasal patency were computed [10–13], Nasal resistance ($R = \frac{\Delta P}{Q}$) was defined as the ratio of the transnasal pressure drop from nostrils to choana (ΔP) in Pa to the volume flowrate (Q) in ml/s. Heat flux per unit time and area (units of W/m^2), which is the rate of heat loss across the nasal mucosa during inspiration, was calculated as $\phi = -k\nabla T$, where $k = 0.0268 \text{ W}/\text{m}\cdot\text{K}$ is the specific heat of air and ∇T is the temperature gradient at the wall. The surface area stimulated by mucosal cooling was defined as the mucosa surface area where heat flux exceeds $50 \text{ W}/\text{m}^2$ (SAHF50) based on the study by Sullivan and colleagues [11], Airflow partitioning, which is a measure of flow symmetry between the left and right nostrils, was defined as unilateral airflow divided by bilateral airflow.

Airspace cross-sectional areas were computed perpendicular to the main flow direction using the method developed by Garcia and coauthors [51], Briefly, ten streamlines that characterize the main flow direction were identified by selecting release points at the nostril (Fig. 3A). Unilateral cross-sectional areas were computed perpendicular to each streamline in the anterior nose and perpendicular to the nasal floor in the posterior nose. The area vs. distance curve was obtained by averaging the results from the ten streamlines. The minimal cross-sectional area (mCSA) of each nasal cavity was defined as the smallest mCSA among the ten streamlines studied [51].

¹This inlet boundary condition should be distinguished from a flat velocity profile imposed at the nostrils, which has been shown to yield less accurate results than a pressure boundary condition imposed at a spherical surface in front of the face [48]. Here, a pressure boundary condition (not a flat velocity profile) is applied at the nostrils. For a given mesh size, truncation of the geometry at the nostrils provides a higher mesh density inside the nasal passages, which is expected to provide greater accuracy.

Normative ranges

For each CFD variable, we calculated lower and upper limits of the normative range expected to represent 95% of the healthy population. For a Gaussian distribution, the upper and lower bounds would be the average value ± 1.96 times the standard deviation (mean ± 1.96 SD). In this study, rather than assuming a Gaussian distribution, a non-parametric method that utilizes interpolation between appropriate order statistics constructed from the observations was applied to estimate the lower and upper limits of the normative range [52]. Standard errors for the end points of these ranges were calculated using the formula for quantiles [Equation 13 in [52]] using a Gaussian density assumption for this purpose.

RESULTS

Inter-individual variability in nasal cavity morphology

Substantial inter-individual variability in nasal morphology was observed (Figs. 1 and S1; Table S2). The average volume of the nasal cavity was 21.5 ± 4.4 ml and the average surface area was 189 ± 23 cm², respectively. These values represent both nasal cavities together from nostrils to nasal choana, excluding the paranasal sinuses. Volume and surface area significantly correlate with each other (Pearson $r = 0.69$; P value $< 10^{-5}$).

Unilateral cross-sectional areas were similar in the left and right cavities after averaging among the 47 healthy subjects (Fig. 3B). The smallest cross-section of the nasal airspace was located in the anterior 3 cm of the nose in nearly all (89 out of 94) nasal cavities studied (Fig. 3D). The unilateral minimal cross-sectional area was on average 0.66 ± 0.21 cm² (Fig. 3C; Table S3). If we define the “narrow side” as the nasal cavity with the smallest mCSA and the “non-narrow side” as the contralateral cavity in each patient, the average mCSA was 0.57 ± 0.18 cm² in the narrow side and 0.75 ± 0.19 cm² in the non-narrow-side.

Normative range of biophysical variables

The normal range for unilateral airflow in healthy adults was found to be 60 ± 20 to 191 ± 20 ml/s (Table 1). Airflow partitioning had a normative range from $(23.8 \pm 7.8)\%$ to $(76.2 \pm 7.8)\%$. The area-weighted-average unilateral heat flux from nostrils to choana had a normative range from 94 ± 29 to 281 ± 58 W/m². The normal range for stimulated surface area (SAHF50) was 27.4 ± 7.4 to 64.3 ± 4.6 cm². Unilateral nasal resistance had a normative range from 0.029 ± 0.011 to 0.32 ± 1.32 Pa.s/ml. The normal range for bilateral nasal resistance was 0.017 ± 0.004 to 0.12 ± 0.13 Pa.s/ml. The unilateral airspace mCSA had a normative range from 0.24 ± 0.15 to 1.21 ± 0.68 cm² (Table 1; Table S4).

Resistance profile

To investigate inter-individual variability in regional resistance, each nasal cavity was sectioned into 6 coronal cross-sections and every section was tagged in relation to their relative distance from the nostril, as defined by $D = H/L_{\text{septum}}$, where H is the distance from the nostrils and L_{septum} is the septal length. The most posterior extent of either nostril was designated as relative distance $D=0$ and the posterior-most edge of the septum as $D=1.0$ (Fig. 4). The bilateral pressure drop was largest in the nasal valve region (regions 1 and 2 in

Fig. 4). The pressure drop in the posterior turbinate region (regions 5 and 6 in Fig. 4) was relatively small as compared to the nasal valve region.

Intranasal airflow distribution

Intranasal airflow distribution in healthy individuals was studied in 5 uniformly-spaced coronal sections (Fig. 5). Each coronal section was subdivided into inferior, middle, and superior regions, each region corresponding to exactly 1/3 of the height of the nasal cavity at that location. The percentage of total unilateral flow allocated to each region was found to be $(37\pm 17)\%$ in the inferior region, $(51\pm 12)\%$ in the middle region, and $(12\pm 8)\%$ in the superior region, averaged for the 5 coronal cross-sections in Figure 5. There was a tendency for posterior sections to have less inferior airflow and more middle and superior airflows (Fig. 5B). Middle airflow and inferior airflow were significantly correlated with total unilateral airflow, but superior airflow did not correlate significantly with unilateral airflow (Fig. 5C). This implies that the percentage of inhaled air that reaches the olfactory cleft is not a constant percentage of unilateral flowrate in different individuals, but rather depends strongly on the anatomy of each individual.

DISCUSSION

Currently, NAO surgical planning relies on subjective symptoms, clinical exam findings, and surgeon judgment without objective measurements of nasal airflow [2,53]. Many studies have quantified the minimal cross-sectional area of the nasal airspace via acoustic rhinometry and nasal resistance via rhinomanometry. Although normal ranges of these variables are available in the literature [54,55] and have been adopted by some surgeons as a criterion to select patients for surgery [7], most otolaryngologists have not adopted acoustic rhinometry and rhinomanometry in their surgical planning in part because these objective measures correlate poorly with subjective nasal patency [2]. There is growing evidence that the physiological mechanism of nasal airflow sensation is not resistance to airflow, but mucosal cooling via stimulation of menthol-sensitive TRPM8 cold receptors [8,10,11,56–9]. Quantifying mucosal cooling *in vivo* is challenging [9], but CFD measures of mucosal cooling have been shown to correlate with subjective nasal patency [10–12,57]. The normative ranges reported in Table 1 may be used to identify patients whose airflow variables fall within 95% of the healthy population, which will be particularly important in future CFD-based virtual surgery planning software [16,36,37]. Virtual surgery planning may help reduce the failure rate of NAO surgery, which currently can be greater than 50% in long-term studies [33,35].

The objective of this study was to quantify healthy ranges of CFD variables known to correlate with subjective nasal patency [10–13]. A cohort of 47 healthy subjects with no history of nasal obstruction, and no evidence of sinus disease on CBCT scans was studied. The absence of NAO symptoms in this healthy cohort was verified with the NOSE questionnaire (all subjects had NOSE score < 32). This is important because CBCT findings are often inconsistent with subjective symptoms. Average NOSE and VAS scores in our cohort were 5 ± 7 and 1.1 ± 1.8 respectively, which are within the ranges reported for asymptomatic subjects in a recent systematic literature review (NOSE = 15 ± 17 and VAS =

2.1 ±1.6) [29], The inclusion criterion (NOSE score < 32) was based on the NOSE scale because it is a validated disease-specific instrument for NAO. The visual analog scale (VAS) was also obtained and reported for completeness. Previous studies from our group found that CFD measures of nasal airflow correlate with both NOSE and VAS scores [10–13], The correlation coefficients are somewhat higher with the NOSE score, but the VAS score also has a robust correlation with CFD variables.

The wide degree of inter-individual variability in nasal anatomy and nasal airflow in our study is supported by previous *in vivo* studies. First, the minimal cross-sectional area estimated in our study is in good agreement with acoustic rhinometry measurements. Based on a recent literature review [51], most acoustic rhinometry studies report a unilateral mCSA around 0.70 cm² in healthy subjects. For example, one of the largest cohorts of healthy subjects available in the literature reported a mCSA of 0.73 ± 0.20 cm² in Caucasians [58], This is in good agreement with the average mCSA in our study (0.66 ± 0.21 cm²), which was also based on a cohort of mostly Caucasian subjects, but used a completely different technology to quantify airspace cross-sectional areas (i.e., 3D reconstructions based on CBCT scans and CFD simulations of flow streamlines) [51].

Second, the wide range of airflow partitioning between the left and right nostrils in our study is in good agreement with nasal spirometry measurements reported by Roblin and Eccles [59], These authors reported that the mean nasal partitioning ratio (NPR) in a cohort of 100 healthy volunteers was -0.10 ± 0.32 without mucosal decongestion. NPR was defined as the difference in flowrate between the two nostrils divided by the total flowrate, so that NPR = -1, 0, and +1 correspond respectively to total left-side obstruction, equal flow partitioning between nostrils, and total right-side obstruction. The authors reported that NPR had a Gaussian distribution, so that a 95% reference range may be computed from the mean ± 1.96 SD. Thus, assuming a mean of 0 and standard deviation of 0.32, the reference range of NPR in healthy individuals is [-0.63, +0.63], Using the identity (Airflow Partitioning) = $100 * (\frac{1}{2}) * (1 + NPR)$ to convert the nasal partitioning ratio to the definition of airflow partitioning used in our study, the data from Roblin and Eccles (2003) correspond to a normative range of 18.6% to 81.4%. This is in good agreement with the normative range for airflow partitioning of (23.8±7.8)% to (76.2±7.8)% obtained in our study. This wide range of airflow partitioning between the left and right nostrils of healthy subjects is also supported by research on the nasal cycle [60], Rhinomanometry measurements have shown that 5-fold oscillations in unilateral nasal resistance are observed routinely due to spontaneous changes in mucosal engorgement associated with the nasal cycle [61].

Third, intranasal airflow distribution in our study (inferior flow: 37±17%, middle flow: 51 ±12%, and superior flow: 12±8%) is in good agreement with the CFD results reported by Zhao and Jiang [23], namely inferior flow: 36±12%, middle flow: 48±12%, and superior flow: 16±10%. These results confirm that a small fraction of inhaled air (12% to 16%) reaches the olfactory region. In a recent paper [13], our group compared the intranasal airflow distribution in 15 healthy subjects with 15 NAO patients. We found that NAO patients had significantly less middle airflow in the narrowest nasal cavity, but inferior and superior flows in the narrow side were not statistically different from healthy individuals. These observations suggest that intranasal airflow distribution may be associated with the

feeling of nasal obstruction, and thus it may be an important variable to account for in future virtual surgery planning.

A key contribution of this study are the novel normative ranges for mucosal cooling variables (Table 1), given that there is growing evidence that mucosal cooling is a key mechanism of nasal airflow sensation [9,8], Sullivan and coauthors (2014) demonstrated that the surface area where heat fluxes exceed 50 W/m^2 (SAHF50) correlates with subjective sensation of nasal airflow. In a subsequent study, Dayal and coauthors (2016) applied virtual surgery and CFD simulations to theoretically predict how mucosal cooling would be affected by complete resection of the inferior turbinate. The CFD simulations revealed that complete resection of the inferior turbinate decreases nasal resistance, but also reduces SAHF50 [62], These findings are consistent with the paradoxical sensation of nasal obstruction in empty nose syndrome (ENS) patients who complain of nasal obstruction after aggressive nasal surgery despite having a normal resistance to airflow [63], In the future, virtual surgery planning based on CFD may help surgeons minimize the risk that patients will develop complications such as ENS after nasal surgery.

To date, standardized CFD methods for NAO surgical planning have not been established. We selected numerical methods (steady-state, laminar simulations, constant wall temperature, planar nostrils with pressure boundary conditions) that minimize computational time, which will be an important factor in future clinical application of virtual surgery planning tools. We expect that the normative ranges reported in Table 1 will be sensitive to some numerical settings, but insensitive to others. For example, adoption of a laminar model rather than a turbulence model is expected to have a minor impact on the normative ranges, given that at low breathing rates laminar simulations are in excellent agreement with experiments [22], In contrast, the radiodensity threshold used to segment the nasal anatomy is known to have a major impact on CFD estimates of nasal airflow [64,65], A recent study found that increasing the radiodensity threshold from -800 HU to -300 HU resulted in a 2-fold reduction in nasal resistance [64], Therefore, application of the normative ranges reported in Table 1 requires adoption of the -300 HU segmentation threshold and other numerical methods used to derive them. We demonstrated previously that CFD variables computed with these numerical methods have a good correlation with subjective nasal patency [10–13], Thus, the normative ranges reported in Table 1 are a valid approach for NAO virtual surgery planning, but certainly not the only one.

The high degree of inter-individual variability in nasal airflow variables (Table 1) (and also intra-individual variability due to the nasal cycle [60]) presents a major challenge to adoption of objective measures of nasal airflow into clinical care [66], Some overlap is expected between the ranges of nasal airflow variables in healthy subjects and patients with NAO. For example, the healthy range for SAHF50 was found to be 27.4 to 64.3 cm^2 (Table 1). In an earlier study of 10 patients with NAO [11], we found that SAHF50 ranged from 13.2 to 42.7 cm^2 , which overlaps with the normative range. In this small cohort of NAO patients, 4 out 10 patients had $\text{SAHF50} < 25 \text{ cm}^2$, 6 out 10 patients had $\text{SAHF50} < 35 \text{ cm}^2$, and 10 out 10 patients had $\text{SAHF50} < 43 \text{ cm}^2$. Therefore, the sensitivity of SAHF50 to identify NAO patients is 40%, 60%, or 100% depending on the threshold value applied. Future studies should compare CFD variables in NAO patients with the normative ranges in

Table 1 and thus determine how best to implement these normative ranges in surgical planning.

Some limitations of this study must be acknowledged. First, some subjects in our cohort showed evidence of nasal cycling. Fluctuations in mucosal engorgement associated with the nasal cycle represent a considerable challenge when investigating objective measures of nasal airflow [12,66–68]. In the acoustic rhinometry and rhinomanometry literature, mucosal decongestion is often used to abolish the effect of the nasal cycle. In our study, the CBCT scans were collected without mucosal decongestion because our goal was to quantify nasal physiology in its natural state. Additional studies are needed to quantify intra-individual variability in nasal airflow during the nasal cycle. Second, most subjects in our sample were Caucasian. Future studies need to investigate inter-individual variability in nasal anatomy due to race. Finally, only adult subjects were included in our study. Additional studies are needed to develop normative ranges of nasal airflow for pediatric populations.

Another limitation of this study is the manual segmentation of the paranasal sinuses, which implies some degree of subjectivity in the creation of the 3D models. For consistency, the 3D reconstructions of all 47 healthy subjects were created by the same engineer (Borojeni) and checked by another engineer with extensive experience in nasal anatomy (Garcia) and by a board-certified otolaryngologist (Rhee). The ostia of the maxillary sinuses and sphenoid sinuses are well-defined, thus there is minimal subjectivity in excluding these two sinuses. In contrast, the ostia of the frontal and ethmoidal sinuses are less defined, thus their exclusion leads to some subjectivity in variables such as the volume and surface area of the nasal passages. Fortunately, this subjectivity in defining the boundaries of the paranasal sinuses is expected to have a negligible effect on the key CFD variables reported in our study (nasal resistance, airspace minimal cross-sectional area, airflow partitioning between the left and right nostrils, and heat flux measures). These key CFD variables are determined primarily by nasal resistance, which in turn is determined primarily by the geometry of the anterior nose (nasal valve region) [51,69]. Since the ostia of the frontal and ethmoidal sinuses are not located in the nasal valve region, but rather are located in the middle meatus, exclusion of the paranasal sinuses is expected to have a minimal effect on these key CFD variables.

In summary, virtual surgery planning based on CFD simulations of nasal airflow has the potential to improve surgical outcomes for patients with nasal airway obstruction. The aim of this study was to quantify nasal airflow variables in a large cohort of healthy individuals that can serve as targets in future virtual surgery planning. The normative ranges of nasal airflow variables were validated by comparing our CFD predictions to healthy ranges of airflow partitioning and airspace minimal cross-sectional area reported in the rhinomanometry and acoustic rhinometry literature. Future studies should consider possible clinical applications of these normative ranges, such as for diagnosis of nasal airway obstruction and surgical planning. Finally, future studies should also investigate how race and ethnicity affect these normative ranges.

Supplementary Material

Refer to Web version on PubMed Central for supplementary material.

Funding:

National Institute of Biomedical Imaging and Bioengineering (NIBIB)

Grant number: R01EB009557

Funding: This study was funded by grant R01EB009557 from the National Institutes of Health/National Institute of Biomedical Imaging and Bioengineering to the Medical College of Wisconsin (MCW) and by subcontract from MCW to the University of North Carolina at Chapel Hill, Duke University, and Marquette University School of Dentistry.

REFERENCES

- Vogt K, Jalowayski AA, Althaus W, Cao C, Han D, Hasse W, Hoffrichter H, Mosges R, Pallanch J, Shah-Hosseini K, Peksis K, Wernecke KD, Zhang L, Zaporoshenko P (2010) 4-Phase-Rhinomanometry (4PR)-- basics and practice 2010. *Rhinology Supplement* (21):1–50
- Andre RF, Vuyk HD, Ahmed A, Graamans K, Nolst Trenite GJ (2009) Correlation between subjective and objective evaluation of the nasal airway. A systematic review of the highest level of evidence. *Clin Otolaryngol* 34 (6):518–525. doi:10.1111/j.1749-4486.2009.02042.x [PubMed: 20070760]
- Hopkins C (2010) Re: Correlation between subjective and objective evaluation of the nasal airway. *Clin Otolaryngol* 35 (2):147–148; author reply 148. doi:10.1111/j.1749-4486.2010.02102.x [PubMed: 20500587]
- Eccles R, Doddi NM, Leong S (2010) Re: Correlation between subjective and objective evaluation of the nasal airway. *Clin Otolaryngol* 35 (2):149; author reply 150. doi:10.1111/j.1749-4486.2010.02101.x [PubMed: 20500589]
- Williams J, Kulendra K, Hanif J (2010) Re: Correlation between subjective and objective evaluation of the nasal airway. *Clin Otolaryngol* 35 (2):150–151; author reply 151–152. doi:10.1111/j.1749-4486.2010.02107.x [PubMed: 20500590]
- Barnes ML, White PS, Gardiner Q (2010) Re: Correlation between subjective and objective evaluation of the nasal airway. *Clin Otolaryngol* 35 (2):152–153; author reply 153. doi:10.1111/j.1749-4486.2010.02110.x [PubMed: 20500593]
- Holmstrom M (2010) The use of objective measures in selecting patients for septal surgery. *Rhinology* 48 (4):387–393. doi:10.4193/Rhinol.072 [PubMed: 21442073]
- Sozansky J, Houser SM (2014) The physiological mechanism for sensing nasal airflow: a literature review. *Int Forum Allergy Rhinol* 4 (10):834–838. doi:10.1002/alr.21368 [PubMed: 25079504]
- Bailey RS, Casey KP, Pawar SS, Garcia GJ (2017) Correlation of Nasal Mucosal Temperature With Subjective Nasal Patency in Healthy Individuals. *JAMA Facial Plast Surg* 19 (1):46–52. doi: 10.1001/jamafacial.2016.1445 [PubMed: 27918749]
- Kimbell JS, Frank DO, Laud P, Garcia GJ, Rhee JS (2013) Changes in nasal airflow and heat transfer correlate with symptom improvement after surgery for nasal obstruction. *J Biomech* 46 (15):2634–2643. doi:10.1016/j.jbiomech.2013.08.007 [PubMed: 24063885]
- Sullivan CD, Garcia GJ, Frank-Ito DO, Kimbell JS, Rhee JS (2014) Perception of better nasal patency correlates with increased mucosal cooling after surgery for nasal obstruction. *Otolaryngol Head Neck Surg* 150 (1):139–147. doi:10.1177/0194599813509776 [PubMed: 24154749]
- Gaberino C, Rhee JS, Garcia GJ (2017) Estimates of nasal airflow at the nasal cycle mid-point improve the correlation between objective and subjective measures of nasal patency. *Respir Physiol Neurobiol* 238:23–32. doi:10.1016/j.resp.2017.01.004 [PubMed: 28089607]
- Casey KP, Borojeni AA, Koenig U, Rhee JS, Garcia GJ (2017) Correlation between Subjective Nasal Patency and Intranasal Airflow Distribution. *Otolaryngol Head Neck Surg* 156 (4):741–750. doi :10.1177/0194599816687751 [PubMed: 28139171]
- Radulesco T, Meister L, Bouchet G, Varoquaux A, Giordano J, Mancini J, Dessi P, Perrier P, Michel J (2019) Correlations between computational fluid dynamics and clinical evaluation of nasal airway obstruction due to septal deviation: An observational study. *Clin Otolaryngol*. doi: 10.1111/coa.13344

15. Zhao K, Jiang J, Blacker K, Lyman B, Dalton P, Cowart BJ, Pribitkin EA (2014) Regional peak mucosal cooling predicts the perception of nasal patency. *Laryngoscope* 124 (3):589–595. doi: 10.1002/lary.24265 [PubMed: 23775640]
16. Vanhille DL, Garcia GJM, Asan O, Borojeni AAJ, Frank-Ito DO, Kimbell JS, Pawar SS, Rhee JS (2018) Virtual Surgery for the Nasal Airway: A Preliminary Report on Decision Support and Technology Acceptance. *JAMA Facial Plast Surg* 20 (1):63–69. doi:10.1001/jamafacial.2017.1554 [PubMed: 29049474]
17. Sanmiguel-Rojas E, Burgos MA, Esteban-Ortega F (2018) Nasal surgery handled by CFD tools. *International journal for numerical methods in biomedical engineering* 34 (10):e3126. doi:10.1002/cnm.3126 [PubMed: 29968373]
18. Doorly DJ, Taylor DJ, Schroter RC (2008) Mechanics of airflow in the human nasal airways. *Respir Physiol Neurobiol* 163 (1–3):100–110. doi:10.1016/j.resp.2008.07.027 [PubMed: 18786659]
19. Kelly JT, Prasad AK, Wexler AS (2000) Detailed flow patterns in the nasal cavity. *J Appl Physiol* (1985) 89 (1):323–337. doi:10.1152/jappl.2000.89.1.323 [PubMed: 10904068]
20. Kim SK, Chung SK (2004) An investigation on airflow in disordered nasal cavity and its corrected models by tomographic PIV. *Meas Sci Technol* 15 (6):1090–1096. doi:Pii S0957–0233(04)71210–2 10.1088/0957-0233/15/6/007
21. Leong SC, Chen XB, Lee HP, Wang DY (2010) A review of the implications of computational fluid dynamic studies on nasal airflow and physiology. *Rhinology* 48 (2):139–145. doi:10.4193/Rhin09.133 [PubMed: 20502749]
22. Li C, Jiang J, Dong H, Zhao K (2017) Computational modeling and validation of human nasal airflow under various breathing conditions. *J Biomech* 64:59–68. doi:10.1016/j.jbiomech.2017.08.031 [PubMed: 28893392]
23. Zhao K, Jiang J (2014) What is normal nasal airflow? A computational study of 22 healthy adults. *Int Forum Allergy Rhinol* 4 (6):435–446 [PubMed: 24664528]
24. Ramprasad VH, Frank-Ito DO (2016) A computational analysis of nasal vestibule morphologic variabilities on nasal function. *J Biomech* 49 (3):450–457. doi:10.1016/j.jbiomech.2016.01.009 [PubMed: 26830439]
25. Sanmiguel-Rojas E, Burgos MA, Del Pino C, Sevilla-Garcia MA, Esteban-Ortega F (2018) Robust nondimensional estimators to assess the nasal airflow in health and disease. *International journal for numerical methods in biomedical engineering* 34 (1). doi:10.1002/cnm.2906
26. Liu Y, Johnson MR, Matida EA, Kherani S, Marsan J (2009) Creation of a standardized geometry of the human nasal cavity. *J Appl Physiol* (1985) 106 (3):784–795. doi:10.1152/japplphysiol.90376.2008 [PubMed: 19131483]
27. Churchill SE, Shackelford LL, Georgi JN, Black MT (2004) Morphological variation and airflow dynamics in the human nose. *American journal of human biology : the official journal of the Human Biology Council* 16 (6):625–638. doi:10.1002/ajhb.20074 [PubMed: 15495233]
28. Guilmette RA, Cheng YS, Griffith WC (1997) Characterising the variability in adult human nasal airway dimensions. *Annals of Occupational Hygiene* 41:491–497
29. Rhee JS, Sullivan CD, Frank DO, Kimbell JS, Garcia GJ (2014) A systematic review of patient-reported nasal obstruction scores: defining normative and symptomatic ranges in surgical patients. *JAMA Facial Plast Surg* 16 (3):219–225; quiz 232. doi:10.1001/jamafacial.2013.2473 [PubMed: 24604253]
30. Dinis PB, Haider H (2002) Septoplasty: long-term evaluation of results. *American journal of otolaryngology* 23 (2):85–90 [PubMed: 11893975]
31. Dommerby H, Rasmussen OR, Rosborg J (1985) Long-term results of septoplastic operations. *ORL; journal for oto-rhino-laryngology and its related specialties* 47 (3):151–157 [PubMed: 4000654]
32. Fjermedal O, Saunte C, Pedersen S (1988) Septoplasty and/or submucous resection? 5 years nasal septum operations. *J Laryngol Otol* 102 (9):796–798 [PubMed: 3171372]
33. Ho WK, Yuen AP, Tang KC, Wei WI, Lam PK (2004) Time course in the relief of nasal blockage after septal and turbinate surgery: a prospective study. *Archives of otolaryngology--head & neck surgery* 130 (3):324–328. doi:10.1001/archotol.130.3.324 [PubMed: 15023841]

34. Ilium P (1997) Septoplasty and compensatory inferior turbinate hypertrophy: long-term results after randomized turbinoplasty. *Eur Arch Otorhinolaryngol* 254(Suppl 1):S89–92
35. Jessen M, Ivarsson A, Malm L (1989) Nasal airway resistance and symptoms after functional septoplasty: comparison of findings at 9 months and 9 years. *Clinical otolaryngology and allied sciences* 14 (3):231–234 [PubMed: 2743612]
36. Burgos MA, Sanmiguel-Rojas E, Del Pino C, Sevilla-Garcia MA, Esteban-Ortega F (2017) New CFD tools to evaluate nasal airflow. *Eur Arch Otorhinolaryngol* 274 (8):3121–3128. doi:10.1007/s00405-017-4611-y [PubMed: 28547013]
37. Burgos MA, Sanmiguel-Rojas E, Singh N, Esteban-Ortega F (2018) DigBody((R)): A new 3D modeling tool for nasal virtual surgery. *Comput Biol Med* 98:118–125. doi:10.1016/j.combiomed.2018.05.016 [PubMed: 29787939]
38. Hariri BM, Rhee JS, Garcia GJ (2015) Identifying patients who may benefit from inferior turbinate reduction using computer simulations. *Laryngoscope* 125 (12):2635–2641. doi:10.1002/lary.25367 [PubMed: 25963247]
39. Stewart MG, Witsell DL, Smith TL, Weaver EM, Yueh B, Hannley MT (2004) Development and validation of the Nasal Obstruction Symptom Evaluation (NOSE) scale. *Otolaryngol Head Neck Surg* 130 (2):157–163. doi:10.1016/j.otohns.2003.09.016 [PubMed: 14990910]
40. Calhoun KH, Waggenspack GA, Simpson CB, Hokanson JA, Bailey BJ (1991) CT evaluation of the paranasal sinuses in symptomatic and asymptomatic populations. *Otolaryngol Head Neck Surg* 104 (4):480–483. doi:10.1177/019459989110400409 [PubMed: 1903859]
41. Jones NS, Strobl A, Holland I (1997) A study of the CT findings in 100 patients with rhinosinuitis and 100 controls. *Clinical otolaryngology and allied sciences* 22 (1):47–51 [PubMed: 9088680]
42. Min YG, Jung HW, Kim CS (1995) Prevalence study of nasal septal deformities in Korea: results of a nation-wide survey. *Rhinology* 33 (2):61–65 [PubMed: 7569653]
43. Roblin DG, Eccles R (2002) What, if any, is the value of septal surgery? *Clinical otolaryngology and allied sciences* 27 (2):77–80 [PubMed: 11994109]
44. Vainio-Mattila J (1974) Correlations of nasal symptoms and signs in random sampling study. *Acta Otolaryngol Suppl* 318:1–48 [PubMed: 4528492]
45. Stewart MG, Smith TL, Weaver EM, Witsell DL, Yueh B, Hannley MT, Johnson JT (2004) Outcomes after nasal septoplasty: results from the Nasal Obstruction Septoplasty Effectiveness (NOSE) study. *Otolaryngol Head Neck Surg* 130 (3):283–290. doi:10.1016/j.otohns.2003.12.004 [PubMed: 15054368]
46. Borojeni AA, Frank-Ito DO, Kimbell JS, Rhee JS, Garcia GJM (2017) Creation of an idealized nasopharynx geometry for accurate computational fluid dynamics simulations of nasal airflow in patient-specific models lacking the nasopharynx anatomy. *Int J Numer Meth Bio* 33 (5):e2825. doi:10.1002/cnm.2825
47. Garcia GJ, Bailie N, Martins DA, Kimbell JS (2007) Atrophic rhinitis: a CFD study of air conditioning in the nasal cavity. *J Appl Physiol* (1985) 103 (3):1082–1092. doi:10.1152/japplphysiol.011118.2006 [PubMed: 17569762]
48. Taylor DJ, Doorly DJ, Schroter RC (2010) Inflow boundary profile prescription for numerical simulation of nasal airflow. *J R Soc Interface* 7 (44):515–527. doi:10.1098/rsif.2009.0306 [PubMed: 19740920]
49. Lindemann J, Leiacker R, Rettinger G, Keck T (2002) Nasal mucosal temperature during respiration. *Clinical otolaryngology and allied sciences* 27 (3):135–139 [PubMed: 12071984]
50. Garcia GJ, Schroeter JD, Segal RA, Stanek J, Foureman GL, Kimbell JS (2009) Dosimetry of nasal uptake of water-soluble and reactive gases: a first study of interhuman variability. *Inhalation toxicology* 21 (7):607–618. doi:10.1080/08958370802320186 [PubMed: 19459775]
51. Garcia GJ, Hariri BM, Patel RG, Rhee JS (2016) The relationship between nasal resistance to airflow and the airspace minimal cross-sectional area. *J Biomech* 49 (9):1670–1678. doi:10.1016/j.jbiomech.2016.03.051 [PubMed: 27083059]
52. Troendle JF, Yu KF (2003) Estimation of sample size for reference interval studies. *Biometrical Journal* 45 (5):561–572
53. Chandra RK, Patadia MO, Raviv J (2009) Diagnosis of nasal airway obstruction. *Otolaryngologic clinics of North America* 42 (2):207–225, vii. doi:10.1016/j.otc.2009.01.004 [PubMed: 19328887]

54. Merkle J, Kohlhas L, Zadoyan G, Mosges R, Hellmich M (2014) Rhinomanometric reference intervals for normal total nasal airflow resistance. *Rhinology* 52 (4):292–299. doi:10.4193/Rhin13.220 [PubMed: 25479205]
55. Corey JP, Gungor A, Nelson R, Liu X, Fredberg J (1998) Normative standards for nasal cross-sectional areas by race as measured by acoustic rhinometry. *Otolaryngol Head Neck Surg* 119 (4): 389–393. doi :10.1016/SO194-5998(98)70085-3 [PubMed: 9781997]
56. Burrow A, Eccles R, Jones AS (1983) The effects of camphor, eucalyptus and menthol vapour on nasal resistance to airflow and nasal sensation. *Acta Otolaryngol* 96 (1–2):157–161. doi: 10.3109/00016488309132886 [PubMed: 6613544]
57. Zhao K, Blacker K, Luo Y, Bryant B, Jiang J (2011) Perceiving nasal patency through mucosal cooling rather than air temperature or nasal resistance. *PLoS One* 6 (10):e24618. doi :10.1371/journal.pone.0024618 [PubMed: 22022361]
58. Lenders H, Pirsig W (1990) Diagnostic value of acoustic rhinometry: patients with allergic and vasomotor rhinitis compared with normal controls. *Rhinology* 28 (1):5–16 [PubMed: 2336526]
59. Roblin DG, Eccles R (2003) Normal range for nasal partitioning of airflow determined by nasal spirometry in 100 healthy subjects. *American journal of rhinology* 17 (4):179–183 [PubMed: 12962185]
60. Eccles R (2000) Nasal airflow in health and disease. *Acta Otolaryngol* 120 (5):580–595 [PubMed: 11039867]
61. Hasegawa M, Kern EB (1978) Variations in nasal resistance in man: a rhinomanometric study of the nasal cycle in 50 human subjects. *Rhinology* 16 (1):19–29 [PubMed: 635366]
62. Dayal A, Rhee JS, Garcia GJ (2016) Impact of Middle versus Inferior Total Turbinectomy on Nasal Aerodynamics. *Otolaryngol Head Neck Surg*. doi:10.1177/0194599816644915
63. Moore EJ, Kern EB (2001) Atrophic rhinitis: a review of 242 cases. *American journal of rhinology* 15 (6):355–361 [PubMed: 11777241]
64. Cherobin GB, Voegels RL, Gebrim E, Garcia GJM (2018) Sensitivity of nasal airflow variables computed via computational fluid dynamics to the computed tomography segmentation threshold. *PLoS One* 13 (11):e0207178. doi:10.1371/journal.pone.0207178 [PubMed: 30444909]
65. Quadrio M, Pipolo C, Corti S, Messina F, Pesci C, Saibene AM, Zampini S, Felisati G (2016) Effects of CT resolution and radiodensity threshold on the CFD evaluation of nasal airflow. *Med Biol Eng Comput* 54 (2–3):411–419. doi:10.1007/s11517-015-1325-4 [PubMed: 26059996]
66. Moore M, Eccles R (2012) Normal nasal patency: problems in obtaining standard reference values for the surgeon. *J Laryngol Otol* 126 (6):563–569. doi:10.1017/S002221511200045X [PubMed: 22494413]
67. Patel RG, Garcia GJ, Frank-Ito DO, Kimbell JS, Rhee JS (2015) Simulating the nasal cycle with computational fluid dynamics. *Otolaryngol Head Neck Surg* 152 (2):353–360. doi : 10.1177/0194599814559385 [PubMed: 25450411]
68. Flanagan P, Eccles R (1997) Spontaneous changes of unilateral nasal airflow in man. A reexamination of the ‘nasal cycle’. *Acta Otolaryngol* 117 (4):590–595 [PubMed: 9288218]
69. Haight JS, Cole P (1983) The site and function of the nasal valve. *Laryngoscope* 93 (1):49–55 [PubMed: 6823174]



Fig. 1 -

Coronal sections of 15 nasal cavities located at relative distance $D=0.5$ illustrating inter-subject variability in nasal morphology among healthy subjects. The relative distance D is defined as the ratio of distance from the nostrils to the septum length from the nostrils to the nasal choana. The color boundaries are the outlines of the 3-dimensional nasal cavity models. The cross-sections of the remaining 32 subjects are illustrated in Figure S1 of the Electronic Supplementary Material.

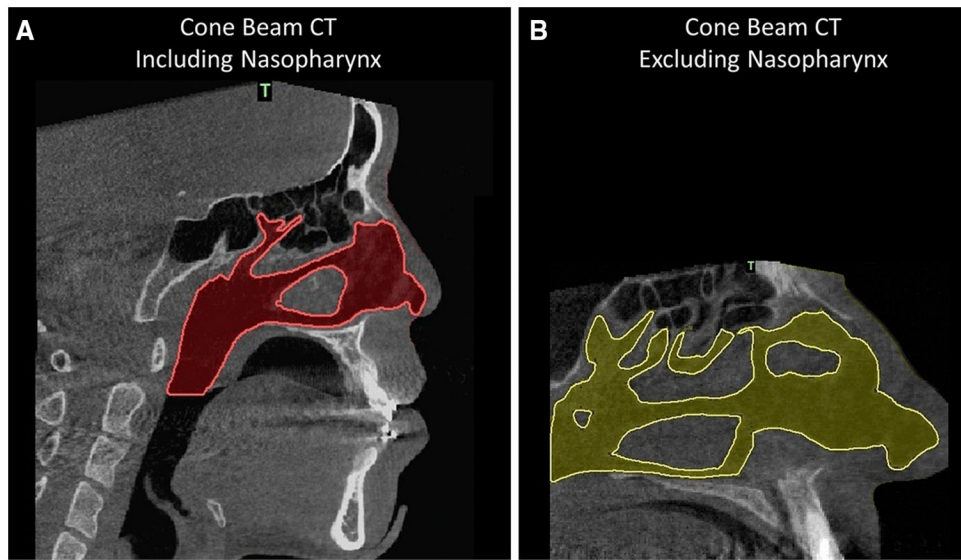


Fig. 2 -
(A) Cone beam computed tomography (CBCT) scan including the nasopharynx. (B) CBCT scan excluding the nasopharynx.

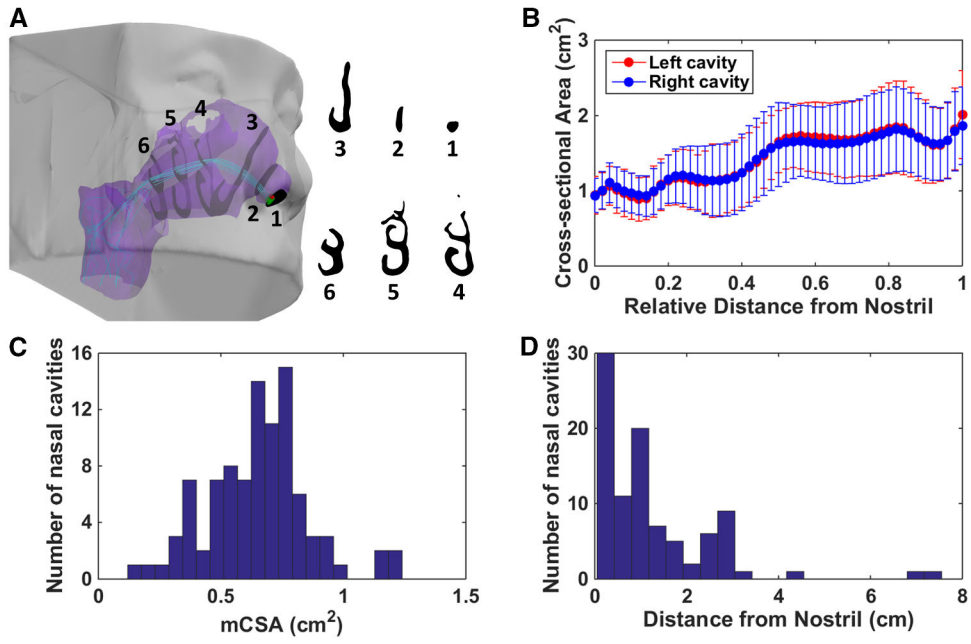


Fig. 3 - Unilateral cross-sectional areas of the nasal airspace in a cohort of 47 healthy individuals. (A) Cross-sectional areas were computed perpendicular to the main flow direction. (B) Average cross-sectional areas of the left cavity and right cavity plotted against the relative distance from nostrils measured along flow streamlines. (C) Histogram of unilateral minimal cross-sectional area (mCSA) for the 94 nasal cavities studied. (D) Histogram of the mCSA location for the 94 nasal cavities studied.

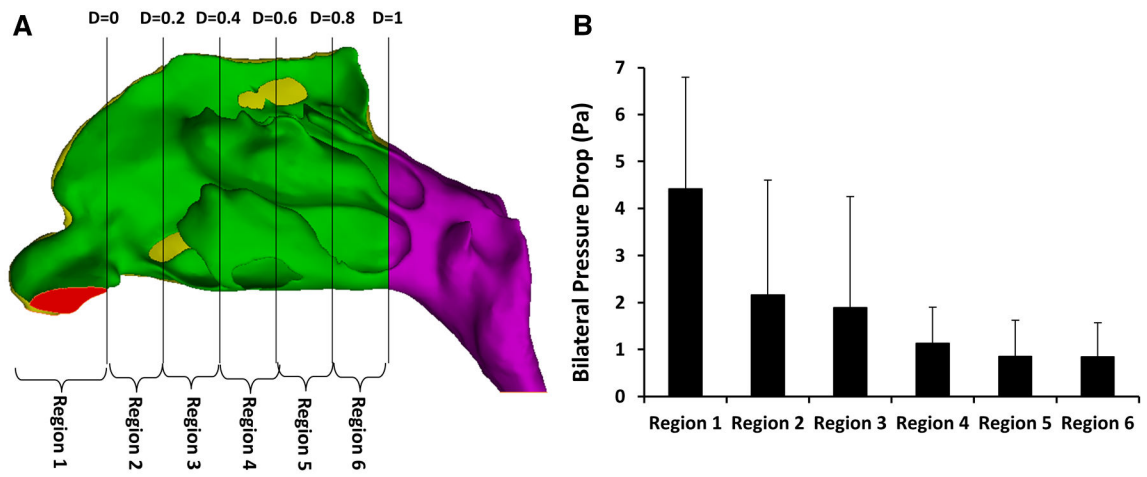


Fig. 4 -
(A) Three-dimensional reconstruction of the nasal cavity displaying definition of 6 regions from nostrils to choana. (B) Regional pressure drop in simulations with 250 ml/s of bilateral airflow.

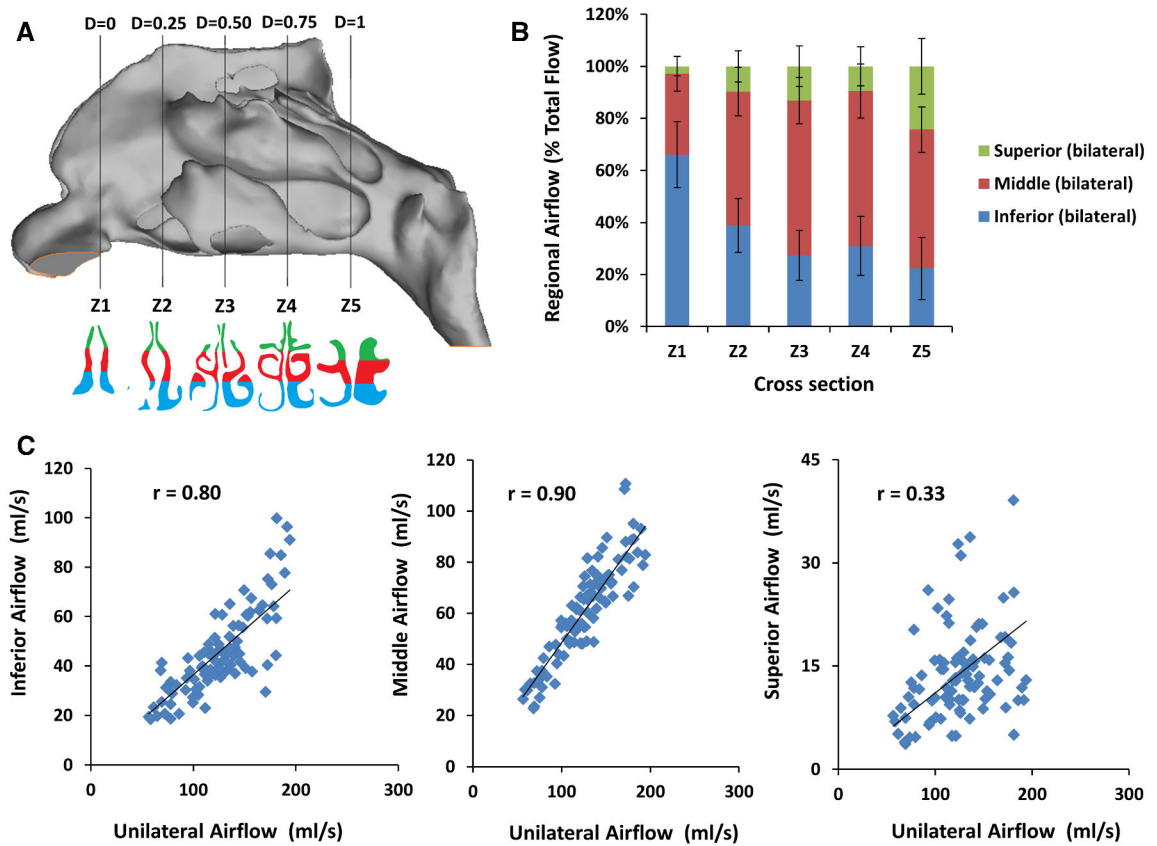


Fig. 5 - Intranasal airflow distribution. (A) Lateral view of the nasal cavity displaying the location of 5 coronal cross sections. (B) Flow allocation to inferior, middle and superior regions at the 5 coronal cross sections. (C) Correlation of regional airflow (averaged over the 5 coronal sections) to total unilateral airflow.

Table 1 -

Normative ranges of nasal airflow variables calculated from pressure-driven CFD simulations with a bilateral flowrate of 250 ml/s. Symbol \pm denotes the 90% confidence interval (CI) of each endpoint of the normative range.

Nonparametric normative values of CFD variables	Bilateral flowrate Q = 250 ml/s	
	Lower limit of normative range	Upper limit of normative range
Unilateral Airflow (ml/s)	60 \pm 20	191 \pm 20
Unilateral Airflow Partitioning (%)	23.8 \pm 7.8	76.2 \pm 7.8
Unilateral Heat Flux (W/m ²)	94 \pm 29	281 \pm 58
Unilateral SAHF50 (cm ²)	27.4 \pm 7.4	64.3 \pm 4.6
Unilateral Resistance (Pa.s/ml)	0.029 \pm 0.011	0.32 \pm 1.32
Bilateral Resistance (Pa.s/ml)	0.017 \pm 0.004	0.12 \pm 0.13
Unilateral mCSA (cm ²)	0.24 \pm 0.15	1.21 \pm 0.68

Abbreviations: SAHF50 = surface area stimulated by mucosal cooling defined as the mucosa surface area where heat fluxes exceed 50 W/m²; mCSA = minimal cross-sectional area of the nasal airspace.